IOP Conf. Series: Journal of Physics: Conf. Series **1249** (2019) 012004 doi:10.1088/1742-6596/1249/1/012004

# Video Processing Techniques for the Contactless Investigation of Large Oscillations

**M Civera**[1,4]**, L Zanotti Fragonara**[2] **and C Surace**[3]

1 Dept of Mechanical and Aerospace Engineering, Politecnico di Torino.

Corso Duca degli Abruzzi, 24 Turin 10129 ITALY marco.civera@polito.it

2 School of Aerospace, Transportation and Manufacturing, Cranfield University.

College Rd, Cranfield MK43 0AL UNITED KINGDOM l.zanottifragonara@cranfield.ac.uk

3 Dept of Structural, Building and Geotechnical Engineering, Politecnico di Torino.

Corso Duca degli Abruzzi, 24 Turin 10129 ITALY cecilia.surace@polito.it

**Abstract.** The experimental acquisition of large vibrations presents various technical difficulties. Especially in the case of geometric nonlinearities, dealing with very flexible, very light structures causes minimal variations in mass or stiffness to affect severely the dynamical response. Thus, sensors' added masses change the behaviour of the structure with respect to the unloaded condition. Moreover, the most common tools regularly employed for acquisition in vibration analysis - that is to say, laser vibrometers and accelerometers - are often designed with small amplitudes in mind. Their recordings are known to lack accuracy when the investigated structure undergoes large or very large motions, due to geometrical reasons. Image-based measurement techniques offer a valid solution to this problem. Here, an ensemble of three video processing techniques are benchmarked against each other and tested as viable options for the non-contact dynamic characterisation of slender beam-like structures. The methods have been applied to the case study of an aluminium spar for a highly-flexible airwing prototype and compared to the measurements recorded by a laser velocimeter and several Raspberry PI Inertial Measurement Units (IMUs), which also proved to be minimally invasive.

## 1. Introduction

Large oscillations are known to exceed the structure's range of transverse displacement, here referred to as the *linear limit* of *w*. Once this threshold is crossed, their dynamic behaviour cannot be described by the linear theory of vibrations, and nonlinearities due to higher-order geometric effects are introduced. Since decades, the nonlinear dynamics of such phenomena have been deeply investigated, also experimentally (see e.g. [1]) and a wide literature exists for the topic (for instance, see [2]). In recent years, the research for accurate dynamic models for the large displacement problem has experienced a great revival, particularly for the need to exploit the beneficial properties of such nonlinearities [3] in what are commonly known as *compliant mechanisms*. However, if one is interested in using these nonlinear terms to build a predictive model and run a simulation of it, even small errors in the model cause the estimation error to constantly sum up timestep after timestep until the model becomes rapidly unreliable. This is a well-known issue, particularly evident for nonlinear dynamics. Yet these geometry-related higher-order nonlinear terms of strain are extremely sensitive to even slight changes in the system properties, i.e., mass and stiffness. Thus, the presence itself of physically-attached sensors, which is the most common procedure for experimental acquisitions, may causes not-negligible local variations in the structure-sensors ensemble mass due to their own weight. The effects of these influences on the nonlinear behaviour of the inspected structure have been largely

4 Author to whom any correspondence should be addressed.

overlooked so far. Also, other well-established non-contact measurement techniques fail to follow properly the curvilinear trajectories of such large motions.

To overcome this practical issue, three distinct non-contact, image-based strategies are proposed here to optically investigate the large vibrations of highly-flexible beam-like cantilevered structures. Specifically, one technique for the estimation of instantaneous frequency and two approaches for the estimation of both instantaneous frequency and amplitude are presented. These are, in the same order, an edge detection-based method for the definition of zero crossings along the spar whole resting configuration (referred to hereinafter as the Video Zero Crossing (V0C) method), a Marker Detection (MD) and tracking routine, and an algorithm for pixels' brightness peak picking applied on a thin vertical slice of the video frame – here named Video Virtual Vibrometer (VVV). Also, a minimally-invasive strategy, based on low-cost and low-weight accelerometers, is presented as a further option.

The large deflections of a beam-like spar for a prototype high-aspect-ratio (HAR) wing [4] have been studied. Indeed, recent developments in the aeronautical industry are leading to more flexible air wings, which require a better understanding of the nonlinear components of motion [5] and more and more research effort has been given to the topic in last years (e.g. [6]). All the tests were performed on the spar alone, as, according to the project main goal [7], the skin should transfer all the aerodynamic load to it and maintain its desired aerodynamic shape unaltered.

The rest of the paper is organised as follow. In Section 2, the most widely used hardware options for the dynamic analysis of the geometric nonlinear (accelerometers, laser Doppler and video acquisition) are presented. In Section 3, the wing spar being studied, and the experimental setup are presented in detail. Section 4 describes the three image-based proposals for dynamic investigation and Section 5 reports the experimental results. Finally, in Section 6 conclusions are made.

## 2. Measurement Strategies for Large Deflections

Deflections can be directly measured as displacements or estimated by velocity or acceleration time histories (THs), integrating numerically along time once or twice. In the latter case, laser velocimeter and physically-attached accelerometers are often the default choices. Both strategies are widely used every day in common practice. Nevertheless, some differences in terms of precision do subsist and numerical integration and derivation procedures, while extremely common and widely spread, are not exempt from technical issues; it is well-known [8] that displacement THs obtained from numerical integration generally suffers from both high and (especially) low-frequency spurious contents. No universal nor principled simple procedure is currently established to define the cut-off frequency for the necessary filtering. Selecting a cut-off frequency too low will result in still corrupted data, while too high values would remove actual data along with the numerical errors. The other alternative is nonlinear detrending, by removing a polynomial of order $n$ fitted on the data; this can be proven to be equivalent to the high-pass filtering procedure [8] but it is again case specific and difficult to generalise. Obviously, it must be added that integrated results present a linear drift, which becomes quadratic if the integration process is performed twice to obtain displacements from accelerations, as the constant of integration is not known a priori and can only be estimated. This implies two additional steps for linear detrending to obtain the transverse displacements and velocities. All these procedures can easily be performed in a number of ways to reach good results but, again, may reduce the estimation accuracy. In conclusion, it can be stated that the accuracy of the processed data depends on the accuracy of the integration/derivation procedure and of the filtering and it is obviously lower or at best equal to the one from directly-acquired displacements. The acquisition technologies and their limitations are even more crucial for the exact assessment of large deflections.

### *2.1. Physically-attached accelerometers*

For small deflections, the regime of the spar is linear, and the vertical component of displacement can be safely approximated to the whole displacement. However, in the case of large flapwise deflections,

the actual motion cannot be anymore assumed as a straight vertical line and its curvature must be accounted for. When the spar beam is sufficiently rotated and displaced, the loading conditions are significantly altered, thus causing the insurgence of geometric nonlinearities. Yet, the angle formed by the restoring force with the beam profile at any point at any given instant can be assumed as time-independent (figure 1); hence, the acceleration as measured by attached accelerometers is always implicitly correct; the main problem is that extrapolating the vertical displacement from the recorded time history is not straightforward.

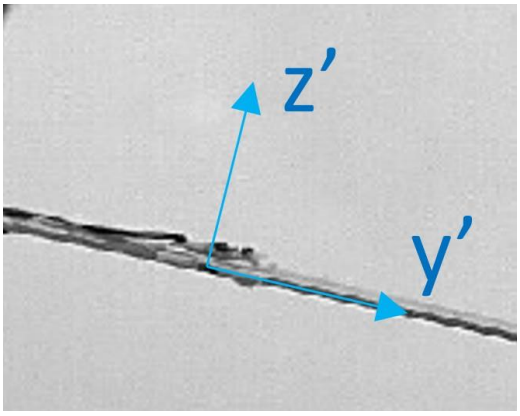


**Figure 1.** Accelerometer's local 2-dimensional reference system *{O,y',z'}* on the focal plane of the camera. Note that *z'* is not parallel to the vertical direction (except at some specific time instants) but is always consistent with the direction of the restoring force.

Other practical issues include that physical sensors need also to remain constrained to the structure all along the test. For very large oscillations, this can mean or to risk having the sensors detaching (especially if they are only glued), or to resort to fixing them, screwing through the beam and thus altering locally not only the mass but also its bending stiffness.

*2.2. Laser Doppler Velocimeter*

The Laser Doppler Velocimeter (or Vibrometer, according to if the transverse displacement $w$ or its time derivative $\dot{w}$ is measured) (LDV) is a widespread mean for the contactless direct measure of speed [9], commonly used for dynamic and modal analyses (see, for instance, [10]); by numerically integrating the velocity THs once, an estimation of the displacements can be produced. Unfortunately, the laser is by definition only sensitive to its direction of application, a straight line ( which is, in this case, applied vertically) passing through an arbitrary point; hence, it is only that component of velocity that is read by the apparatus. For large deflections, the main problem arises from the sliding of the point of application, as can be noticed from the motions depicted in figure 2.d from *P* to *P'*. Due to this effect, the laser velocimeter overestimates the true vertical displacement of point *P*. No hints about horizontal displacement can be obtained, and therefore the reconstruction of the true curvilinear motion of *P* is impossible. Thus, a laser approach is unsuitable for the measurements of large deflections when these transverse displacements exceed a certain range (which is *not necessarily* the linear limit of transverse deflection).

A suitable option would be to resort to tracking laser Doppler vibrometers (TLDVs) [11], to measure local vibrations at a fixed point while the whole surface on which it is contained moves; yet this technique requires a certain knowledge of the expected kinematics of the target point to be tracked and its accuracy depends on the fitness of this mechanical model and the definition of a proper model is not straightforward for the large oscillations problem.

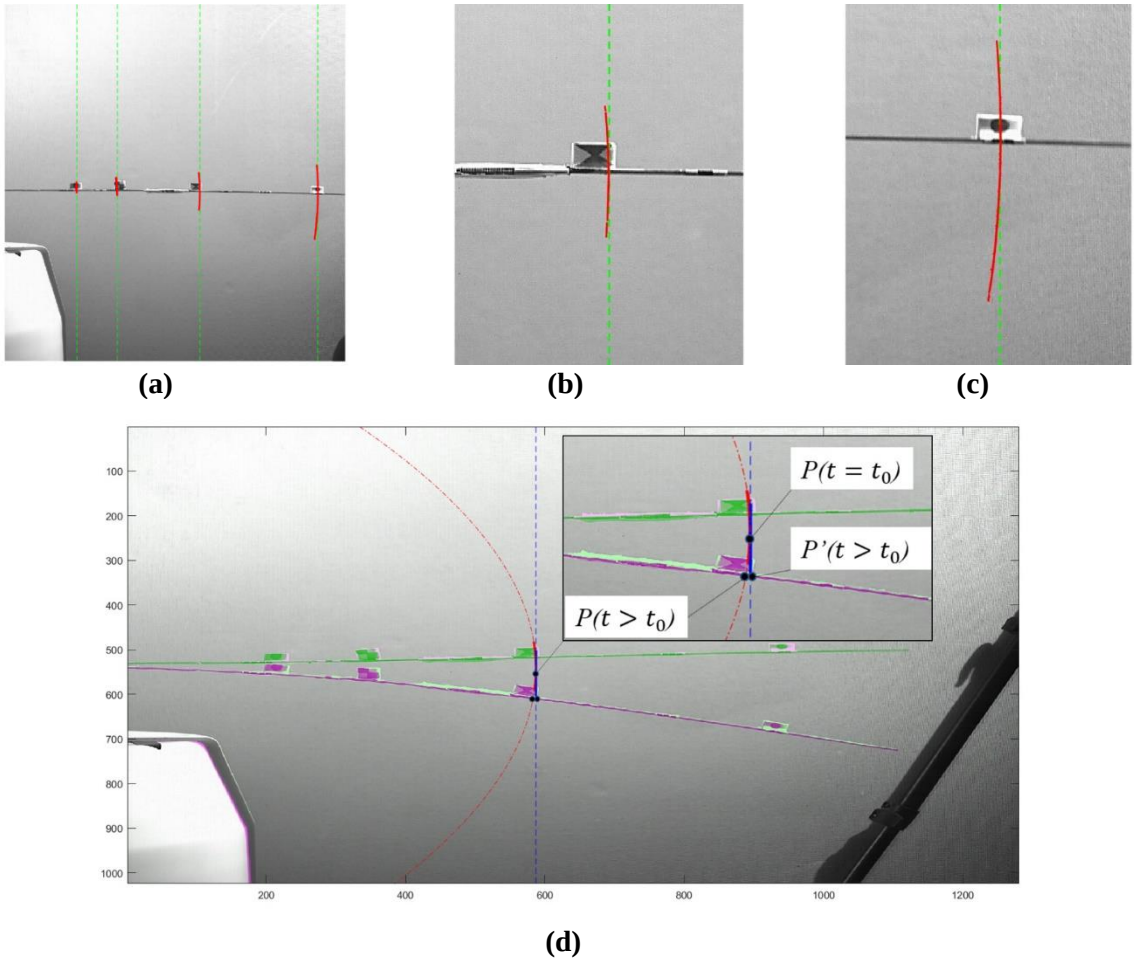


**Figure 2.** Pictorial schematisation of the large deflection issue for non-tracking lasers (side views of the whole spar length **(a)** and zoom around two of the four markers **(b – c)**). The actual curvilinear motion starts to differ clearly from the vertical line tangent to the rest condition at relatively low levels of input excitation, due to the spar high flexibility. **(d)** shows how the cross-section pointed by the laser in the rest condition does not correspond to the one pointed at the extrema (minima and maxima) of deflection.

*2.3. Video Acquisitions*

Recently, a renewed interest in video camera-based acquisition has grown, especially thanks to the new developments in video magnification of small, imperceptible oscillations [12], which have been promptly used as 'virtual' accelerometers [13] and to perform linear modal analysis of simply structures [14]. For larger oscillations, a plethora of vision-based techniques exists and has been applied, e.g., for the Structural Health Monitoring of bridges and other structures; see [15] for instance. A complete review of them will be a paramount task; a review can be found in [16].

## 3. Experimental Setup and Case Study

The beam-like spar comes from the XB-1 prototype studied in [4]. Actually, it can be assumed as a simplified structure for the whole air wing, as it absorbs all the aerodynamic load applied to the wing and, differently from what expected from a standard longeron, it also undergoes torsional rotation around its main axis. Several configurations of sensors and markers were tried; the one of interest is depicted in figure 3.

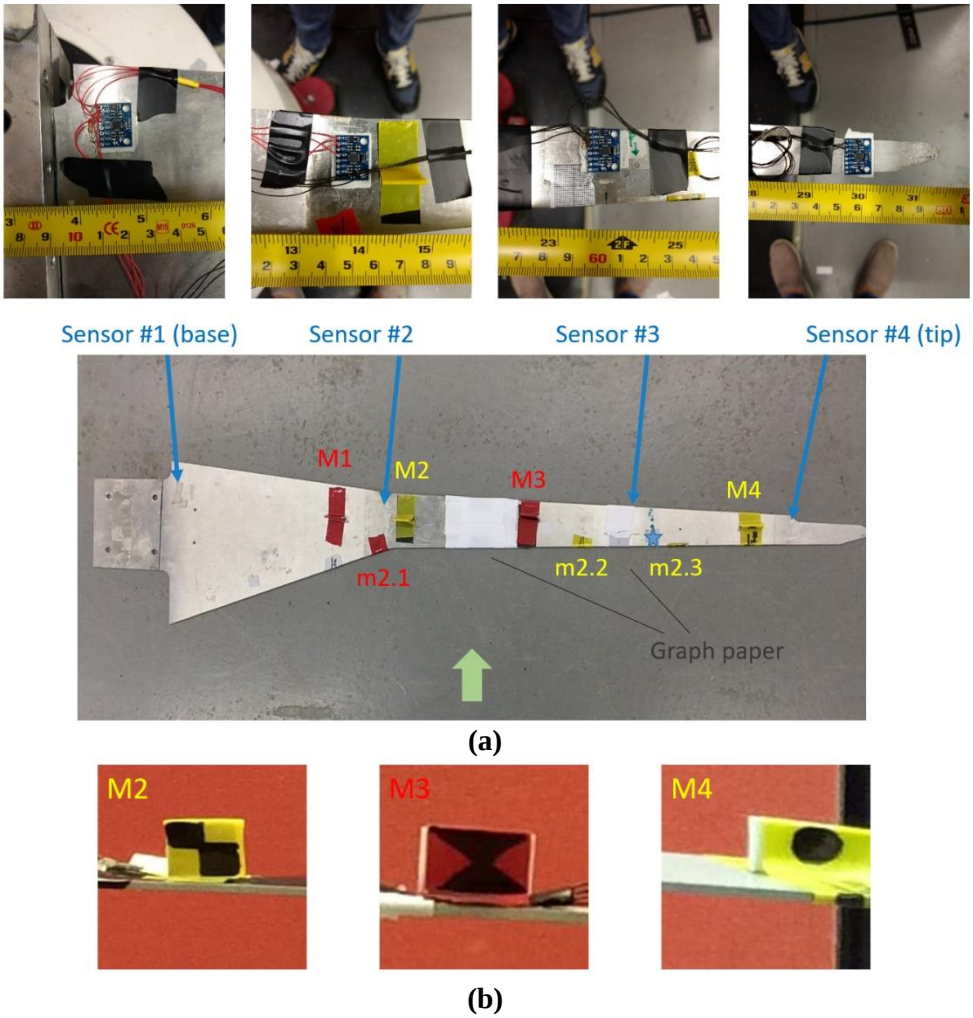


**Figure 3. (a)** top view of the four IMUs sensors for the loaded condition and of the several markers (both attached on the top surface and on the spar profile). **(b)** Markers M1 and M4 were removed during tests with IMUs attached. The light blue star indicates the point of application of the laser in resting condition. The light green arrow indicates the camera point of view (trailing edge).

Experimental data were collected via a Polytec® OFV-505 single point Laser Velocimeter (pointed to the position marked by the light blue start in figure 3.a), four Raspberry Pi ® Inertial Measurement Units (IMUs) and an Olympus ® I-speed 3™ high-speed camera. The Olympus® camera features a global exposure shutter with an exposure time of 1 $\mu$s and a maximum frame rate of 150000 frames per second (fps). The resulting videos were exported in *.hsv* format.
7 markers were considered for the video-based target tracking routine: 3 small ones (m2.1, m2.2 and m2.3) attached on the wing profile and 4 larger ones attached on its extrados (M1, M2, M3 and M4). Their design was purposely differentiated to test the effect on accuracy. M1, not reported in figure 3.b, has the same design as M4 (solid circle) but on a red background. Graph paper was attached in two distinct tracts of the profile for calibration purposes. As it can be seen in (figure 3.a, green arrow), the trailing edge was left in the foreground for video recording, as its motions are *less* apt than the ones of the leading edge to be approximated to be planar and contained in the focal plane. The results proved to have the same accuracy for all the inspected cases. It must be remarked that the study focused on the first normal mode of the air wing, which is purely flexural; hence, no relevant torsion was produced, and the two edges suffered very small or no differential displacements, moving almost at unison.

Two configurations were investigated: with sensors *and* markers (from hereinafter, the *loaded* condition) or with the markers only (*unloaded* condition). Being data from laser, video and accelerometer acquisitions all coming in different features, with different sampling frequencies and accuracies, sensor fusion was needed in order to compare them. All experiments were carried at Cranfield Space Dynamics Laboratory with a Data Physiscs® Signal Force™ modal shaker and its own DP760 close-loop control software.

*3.1. Non-contact measurements: LDV and high-speed camera*

As it can be seen in Figure 2, the zero crossings of the transverse large vibrations always happen at the same spot at which the laser was initially pointed at in rest configuration. Since an area around of the zero can always be linearised (as exploited by the classic 'small displacements' approximation), it is possible to use the laser to measure the frequency of the vibration at the application point, and thus for calling the phase resonance, when input and output signals lag of 90°. This was indeed used to define when to switch on the camera, to start recording while dwelling at resonance or the free decay from resonance (switching the modal shaker off).

Memory capacity is a strong technical issue, as due to this limitation of the camera, any increase in the frame rate (i.e., the number of frames per second fps) is inversely proportional to the maximum duration of the video; the camera has an internal memory capacity limited to 4897 frames, for a 1280 x 1024 pixels wide frame (width x height). Nyquist criterion requires the sampling frequency to be at least the double of the upper bound of the frequency range investigated. More strictly, a common "rule of thumb" is that at least four points per period are necessary to reconstruct faithfully a harmonic oscillation. However, to have a smooth variation of the signal from a sample point to the next one, generally, ten times the highest frequency of interest is needed. This is particularly true for the decay from resonance, where one is interested in obtaining the instantaneous values of both frequency and amplitude, as lower values of sampling frequency $f_{s-\text{video}}$ may miss the amplitude's peaks. Several tests were run; here, only results for 1000 fps are reported. This is almost 10 times higher than the sampling frequency of the IMUs, $f_{s-\text{IMU}}$. Hence, only a few seconds per test were recorded.

A solid red background was used during all recordings. An open-faced lighting fixture with tungsten light source was pointed to it to assure near perfect colour rendition and to avoid any possibility of flickering due to AC fluorescent lights. Regarding the clutter of cables and other attachments in the video, the methods proved to be unaffected by these unrelated movements; nevertheless, it may be misleading if included in the image selected for marker tracking, and cause errors in the other two methodologies.

*3.2. Minimally-invasive measurements: Raspberry Pi ® IMUs*

The four IMUs at disposal have been used both to benchmark the video processing results on the sensor-loaded spar and to test the accelerometers' masses effect on the dynamic response of the same structure, which proved to be minimal, thanks to their very small weight. Their suitability as a low-cost alternative to low weight accelerometers was proved in previous tests and further confirmed here. Since IMUs will short-out if applied directly on a metallic surface, they cannot be mounted with glue or wax; they have rather been applied with a commercial double-sided tape, which proved both to be resistant enough at relatively large accelerations and to not affect the recordings in a perceptible way. The data were then transferred over wi-fi to a Raspberry Pi 2 Model B board. Due to the Raspberry Pi $I^2C$ bus limitation on bit rate, only data sampled at 100 Hz could be sent. This limited the inspectable range of frequency to a maximum of 50 Hz, according to Nyquist's criterion, to avoid aliasing. Mainly for this reason, the whole experiment was limited to the first normal mode of the spar and to its continuation as a nonlinear normal mode for large displacements.

In more detail, IMU breakout boards with Invensense MPU-6050 sensors were used. They provide $I^2C$ interface with internal clock and feature a triple-axis accelerometer and gyroscope, for a total of 6 DoFs per IMU. Thanks to chip configurability, different scales and precision levels can be set for the

gyroscope and accelerometer. They are also equipped with a blinking led, which turned out to be useful for synchronisation with video recorded data during sensor fusion in post-processing. However, being only two $I^2C$ addresses available for MPU-6050 sensors, a second line was needed to collect data simultaneously from all the four chips.

*3.2.1. Effects of the added masses*

It is crucial to remark that, due to gravity, the spar in its rest configuration is not naturally undeflected but starts with an initial curvature $B_0$ under its own weight. This is even increased when sensors are attached to it (figures 4.a and 4.b). As a mean of comparison, the experimental values of the first (linear) natural frequency are reported in Table 1 for some configurations (all data obtained through LDV). 'Black' sensors (figure 4.c) weigh 7 gr each. 'Yellow' ones weigh 24 gr each. Raspberry PI IMUs weigh 2 gr each; the whole apparatus, with 4 IMUs, tape, cables and everything, is slightly less than 11 grams, or less than half a single 'Yellow' accelerometer. Larger markers' weight (figure 3) is almost non-existent, i.e. circa 0.07 gr, all the attachments in the 'unloaded' configuration being slightly less than one and a half the IMUs' weight and scattered all along the spar extrados' surface.

Table 1. first natural frequency for several loading conditions.

| | First natural frequency (Hz) (as a percentage of unloaded condition) |
|---|---|
| No sensor attached (unloaded) | 5.40 Hz (100%) |
| Raspberry PI ® 4 IMUs + cables, tape | 5.36 Hz (99.3%) |
| 1 'black' sensor | 5.23 Hz (96.9%) |
| 2 'black' sensors (same distance from the clamped end) | 5.20 Hz (96.3%) |
| 2 'black' sensors + '2 'yellow' sensors (as depicted in fig. 4) | 4.84 Hz (89.6%) |

It can be easily inferred that, as for damage-related stiffness reduction, the placement of the sensors changes globally the natural frequency of the structure and slightly variates locally the eigenshape of the deflection.

Other relatively low-weight alternatives to accelerometers exist; e.g., strain gauges can be a viable option, but they also do not record directly the vertical displacement; the conversion from strain to displacement may become difficult if, for very large deflections, the nonlinear expression of the curvature from the fixed end becomes necessary [17]. This cannot be rigorously defined a priori, and some sort of double check on the measurements would be therefore needed. Same applies for fibre optics gauges (i.e. Fiber Bragg Grating sensors). While not directly tested, results would most likely confirm what found here for the accelerometers.

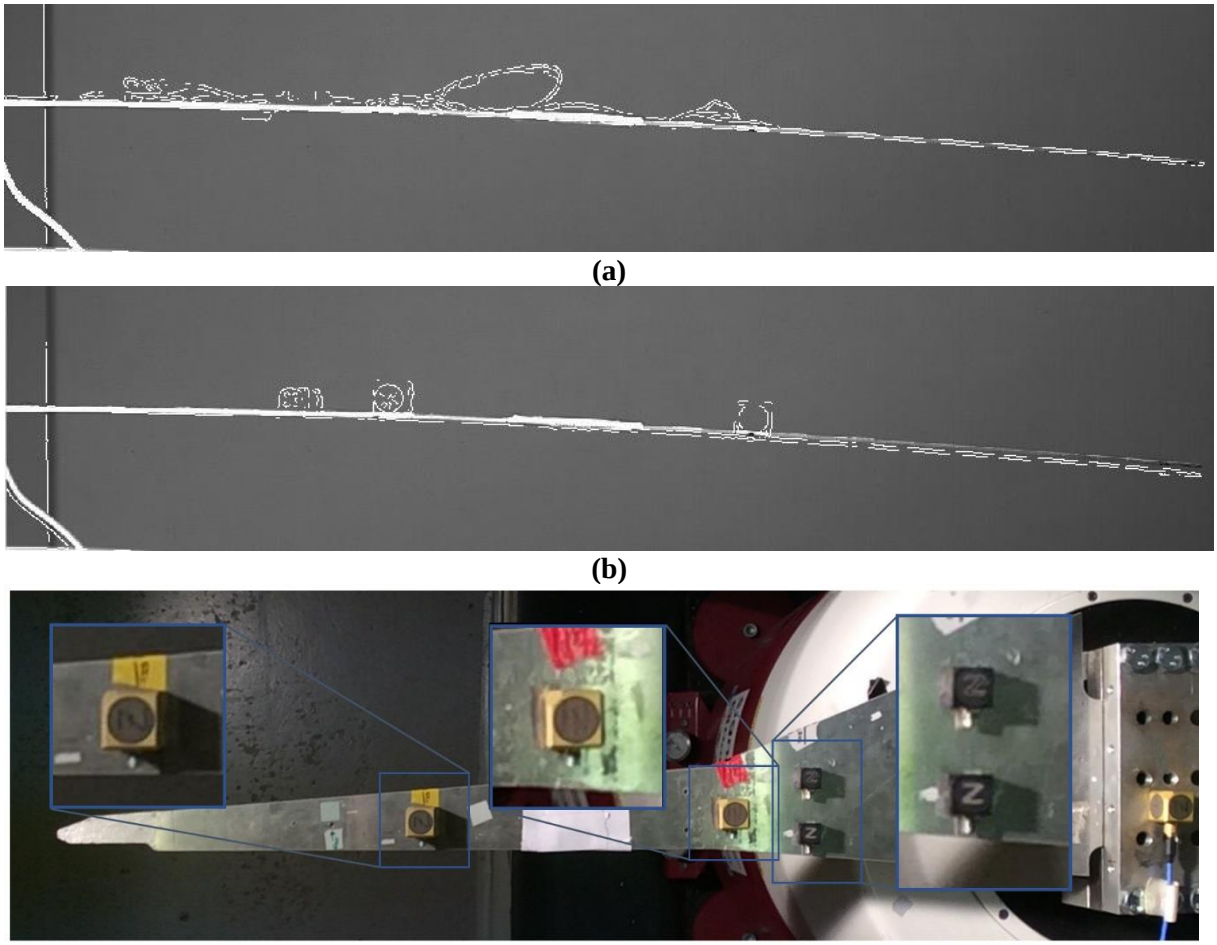

**Figure 4. (a)** unloaded spar with the edges detected from the same structure loaded with 4 IMUs superimposed. The natural deflection in the resting configuration is practically identical. **(b)** Unloaded spar with the edges detected from the same structure loaded with 4 heavier accelerometers superimposed. The static configuration under the resulting weight is significantly different. **(c)** Top view of the two kinds of accelerometers considered: 'Yellow' (left) and 'Black' (right).

## 4. Proposed Video-Based Methods

Out of the three approaches presented here for the task of directly measuring the instantaneous frequency and/or amplitude (pixel-wise) of one or more interest point(s) along the spar trailing edge, Two are Lagrangian, in the sense that they follow a specific feature of a given point along a space (2-D for Marker Detection, 1-D for Virtual Video Vibrometer), and the remaining one is Eulerian, in the sense that it bookkeeps the passages of a feature on a given target position. In all cases, the features are related to image brightness, in different ways. All the methods were implemented in MatLab ®.

### *4.1. Marker Detection (MD) Routine*

The problem presented here is one of multi-target short-term tracking, data-driven (i.e. not model-based), with a single high-speed, high-resolution camera. Some of the most updated advances in the field (as of late 2018) can be found in [18]. To apply the MD algorithm, imperfect, hand-drawn markers were used. In all cases, being the targets relatively far from frame borders, lens distortions were neglected. The process of the Marker Detection routine used here can be briefly defined in 4 simple steps:

1. A frame is (arbitrary) chosen;
2. the machine is presented with a cropped pixel area, large as desired, surrounding the target(s) of interest;
3. Most prominent target features, extracted according to the Speeded-Up Robust Features (SURF) algorithm [19], are automatically enlisted; the selected one(s) are searched for frame-by-frame;
4. Matching points are saved and stored for post-processing.

To speed up the procedure, which can become time-consuming due to the high density of pixels per frame, only a circumscribed area around the position localised in the previous frame was considered for target matching. This is equivalent to assume the interframe movement to be included in that neighbourhood of its previous position. This both reduced dramatically the computational cost of the process and excluded the possibility of blunders, also allowing to use similar and even identical markers, if placed far enough from each other.

Other alternatives were tested on some benchmark video recordings. Specifically, the Binary Robust Invariant Scalable Keypoints (BRISK) [20], the Fusing Points and Lines for High Performance Tracking (FAST) [21], the Harris–Stephens [22], the minimum eigenvalue [23], and the Maximally Stable Extremal Regions (MSER) [24] algorithms were the candidates. In all cases, SURF performed much better than any other feature. The only one slightly comparable were features extracted from MSER, yet they returned much less accurate time histories.

Without going too much into details, the complete algorithm needed to collect the SURF features from a cropped region of the reference frame can be seen as a two-steps approach, based on the Haar wavelet. Firstly, a circular neighbourhood around the point $(x,y)$ of interest in the image $\boldsymbol{I}$ is exploited to identify a reproducible orientation for that point, in order to make the feature detection process invariant (or at least robust) to image rotation. Secondly, a square region, aligned with this dominant direction and centred on the point of interest, is built; the SURF descriptor is then extracted from this region. The size of this square is $20s$, being $s$ the Haar Wavelet filter scale at which the point of interest has been detected. The descriptor vectors are then defined by convolving two Haar wavelet filters of length $2s$ along the x- and y- directions for each one of a certain number of smaller square subregions (by default, $4s$ x $4s$ windows are used), as 4-dimensional vectors $v = (\sum d_x, \sum d_y, \sum |d_x|, \sum |d_y|)$. Thus, the whole descriptor can be summarised as a collection of directional derivatives of the image's brightness; this leads also to sub-pixel accuracy, which was very useful for the aim of this research [25].

The accuracy of the target tracking algorithm depends on several factors, such as (i) the size of the marker, (ii) the marker design, (iii) the spatial resolution (in pixels) of the frame, and (iv) the frame rate, which are identical for the cases reported here. Other parameters of the experimental setup, that is to say, (vi) the exact inclination of the lights (vii) the exact angle and distance of the camera, also suffered minor changes due to having performed the recordings on multiple days. Regarding the reference frame, the resting configuration and the two extrema of deflection of the spar, while dwelling at the first natural frequency, were tested; a detailed discussion is postponed to the Conclusions.

It must be remarked that the invariance to orientation, which is generally utilised to make the algorithm able to recognise the same features from pictures taken from different angles and points of view, is here exploited to recognise the markers when greatly rotated respect to the shape in the target frame. However, in their original paper [19], the authors demonstrated experimentally that the orientation-invariant characteristic of this feature cannot exceed a certain angle. This poses a practical limitation to the amplitude of the marker rotation, hence to the maximum deflection which can be studied. Theoretically, the directional Haar Wavelet Transform guarantees also lighting and contrast

invariance; similar to what experimentally found for the rotational invariance, the algorithm proved to be *robust* to changes in lighting rather than truly *unaffected* by them. Having performed the MD algorithm on all frames (figure 5), plotting the target(s) location throughout them it is possible to define the displacement time histories in terms of pixels and then to convert them to millimetres.

*4.2. Virtual Video Vibrometer (VVV)*

The concept behind the Video Virtual Vibrometer is to exploit the thinness of the air wing profile, reproducing a video-based approach similar to the Laser Doppler Vibrometer and resorting to sharp changes in pixel brightness along a given curve. The curve is here assumed as a vertical straight line, similar to the one actually produced by the laser.

Firstly, the original video frames are converted to 8-bit unsigned integers, that is to say, to grayscale images. Thanks to the sharp contrasts between the background solid red panel and both the upper and lower edges and between the edges themselves and the spar thin profile, a clear M-shaped region arises (figure 5.b). The trend of the pixel brightness reproduced is a mean value over the six columns included into the selected frame slice (green lines in figure 5.a). Following its local minimum allows targeting the 2-mm-thick spar profile enclosed between the two edges. However, the effect of direct illumination on the background panel (which can be easily noticed in figure 5.a) needs to be depurated. Nonlinear detrending can be performed to this aim with any suitable technique. For this particular study, a Savitzky-Golay sliding polynomial filter [26] of order 3 and window width 27 fitted well all the cases investigated (figure 5.c); any other valid alternative applies.

The unsigned integer value of an 8-bit data can range $0-2^8$, that is to say, is upper bound to 256 and cannot assume a negative value. After detrending, a brightness index is here introduced. This value is intended as the negative of the deviation of the brightness from the nonlinear trend applied. The negative is just needed to have the local brightness *minimum* reverted to a local *maximum*, for simplicity. It can also be seen from figure 5 how the presence of other non-moving objects, such as the LDV tripod, can be easily filtered out from the results.

As for the MD algorithm, applying the VVV to all frames produces *vertical* displacement THs for virtually any cross-section of the wing profile. The accuracy of the measurements is inherently non-sub-pixel.

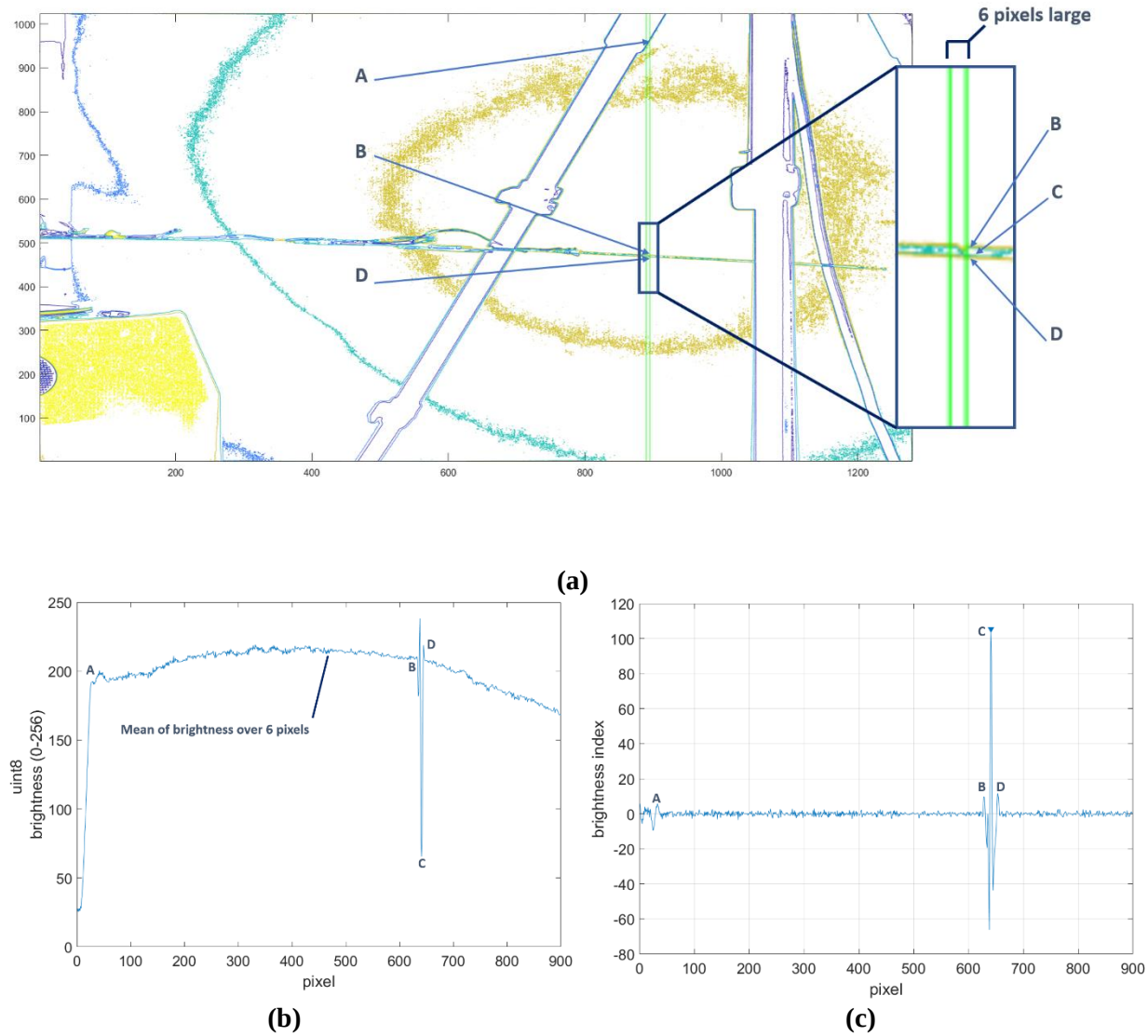


**Figure 5. (a)** Contour plot of pixel brightness in the image frame. The green lines represent the y coordinates of the six-pixel-wide tract of application of the VVV algorithm. **(b)**. The nonlinear trend of pixels' brightness. The local minimum belongs to the 2-mm-thick beam profile enclosed in between the spar extrados and intrados; the global minimum is due to the tripod being included in the vertical slice. **(c)** same mean pixel brightness after automatic nonlinear detrending; peak picking correctly locates the *y* position of the beam profile.

*4.3. Virtual Zero Crossing (V0C)*

Canny edge detection [27] is at the base of the Virtual Zero Crossing approach. Some other edge detection options were tried, such as Sobel', Prewitt' and Roberts' algorithms, to name a few, but Canny algorithm performed always better, as expected from Literature [28]. As for VVV, this technique exploits the thin geometry of the profile on the focal plane. Given a reference frame corresponding to the rest configuration of the spar, only one of the two edges (either the upper or the lower one, with no significant differences) was selected, to have a one-pixel-thick approximation of $B_0$ (figure 6). Afterwards, the algorithm simply bookkeeps, for each pixel considered separately, any frame during which the brightness at that fixed point exceeds an arbitrary threshold. Being the spar more than one pixel thick, the time localisation of zero crossings may be not accurate to the single

frame, as the same passage through the zero could be registered in subsequent frames. Nevertheless, with crossing velocities large enough and an fps rate high enough, the algorithm provided quite good estimations.

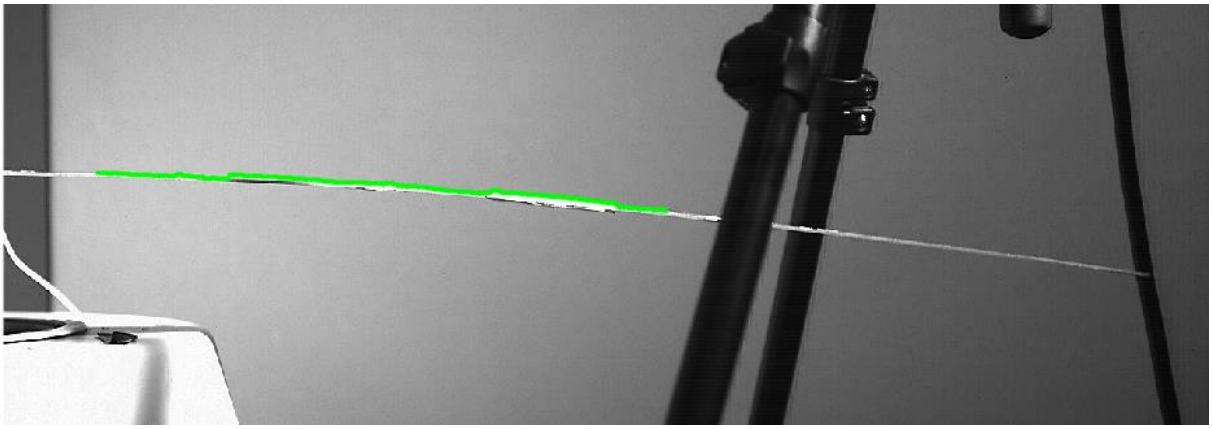

**Figure 6.** The tract of interest the upper edge of the spar (pixels 100 to 700 along the width direction), highlighted and superposed to the reference frame (corresponding to the rest condition of the spar).

## 5. Results and Comparison

Several tests were performed, both inspecting the forced response while dwelling at resonance (for the first natural frequency) and the free decay from this condition. In all cases, phase resonance was called in real-time when the phases of the output (recorded by the laser vibrometer at its point of application) and of the input (recorded by a feedback accelerometer placed on the clamp) were in quadrature; the condition was reached by applying a stepped sweep sine. Data Physics® DP760™ closed-loop control software was used, setting steps of 1 mHz and the automatic settling time option between subsequent steps.

### *5.1. Comparison between the MD routine and the Raspberry PI acquisitions*

Regarding the Marker Detection Algorithm, results for the large markers were overall satisfactory (figure 7), while the smaller ones, painted on the spar profile, gave more mixed results; the quality of the TH extracted from them varied greatly from video to video. All the following discussions will be focused on the larger markers. Some imperfections were still encountered in the THs extracted from them, mainly due to misplaced target detection on some frames. Subpixel fluctuations were also found, resulting in noisy measurements. Overestimation and underestimation divergences were found respect to the THs estimated from the IMUs acquisitions. This can be due to difficulties in locating with high accuracy the larger deflections, where the markers are mostly distorted from their original shape on which the machine has been targeted; it may also be due to the actual different location of markers and sensors (see figure 3.a). Also, IMUs' estimations, while overall reliable, do not match the quality of standard (more expensive) accelerometers; numerical integration of their acceleration THs may amplify these effects.

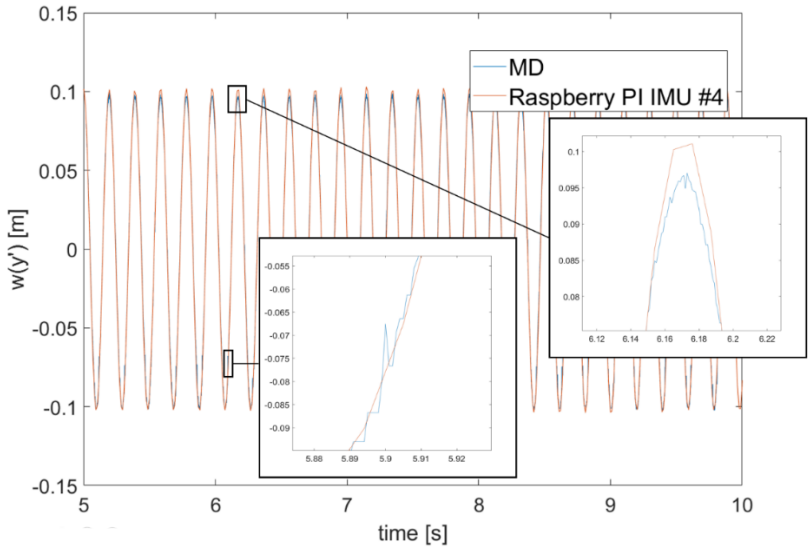


**Figure 7.** Comparison of displacement time histories close to the beam tip dwelling at first natural frequency: Marker M4 (blue line) versus IMU #4 (orange). Note that the frame per second rate of the video camera was ten times larger than the Raspberry PI sampling frequency. Imperfection due to misplaced target detection and underestimation of peak value respect to the TH estimated from IMU recordings are shown in the zoom boxes. This latter effect may also be due to the sensor being closer to the actual beam tip. Measurement noise is also clearly visible in the zoomed tracts.

It was also noticed that the impact of Raspberry PI IMUs' masses on the *linear* dynamic response of the air wing spar was very limited if not totally negligible. If one accepts such a limited error, then Raspberry PI represents a low-cost option for minimally invasive investigation. The effect of the same masses, however, seems to afflict much more the *nonlinear* behaviour of the same structure, and this is currently an object of research for the Authors.

*5.2. Comparison between the MD routine and the VVV algorithm*

The Virtual Video Vibrometer technique showed encouraging results (figure 8). While confounding vertical and curvilinear displacements is theoretically incorrect, this approximation seems to fit quite well for the levels of amplitude here investigated. For small deflections, transversal displacements are almost coincident to their vertical components; at larger amplitudes, they were supposed to diverge more than what encountered; instead, $\Delta w(y')$ and $\Delta v(y')$ seem to remain very similar even for deflections large enough to exceed the linear limit. This may be due to the error for sliding point effect (pictorially described in figure 2.d ) somehow compensating for the error in approximating the curvilinear motion from $P(t_0)$ to $P(t)$ with the distance between $P(t_0)$ and $P'(t)$. However, further investigations are needed in this sense.

To compare MD and VVV it was also necessary to compensate for the distance between the selected feature (on the marker surface) and the spar extrados, $\Delta_{in}$, which was find empirically to remain constant along the whole recording and to be not affected by local motions. From experimental results, the error was always less than 1 mm for deflections up to circa 200 mm, and always in the order of some millimetres for the other larger deflections inspected.

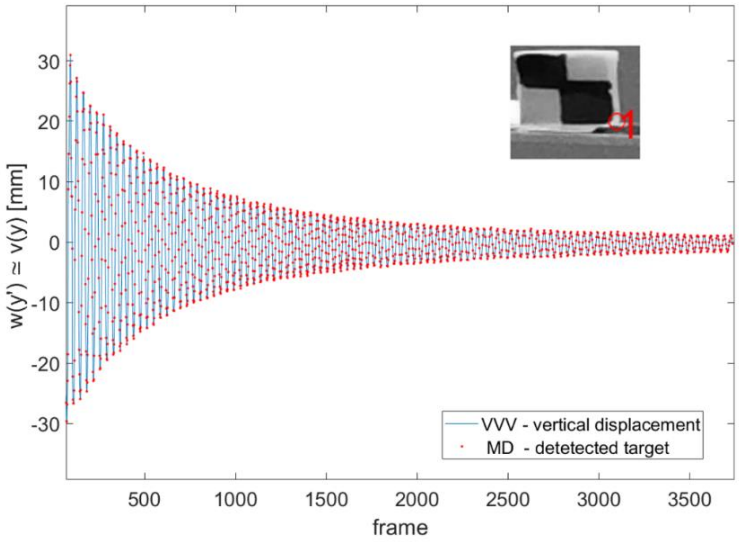


**Figure 8.** Comparison of displacement time histories at the marker M2 in free decay. The specific feature is highlighted in the box in the top right corner. VVV was performed slightly on the right to avoid any interference with the marker.

*5.3. Comparison between the VVV and the V0C algorithms*

Overall. the measurement of instantaneous frequency through V0C was found to be still very noisy, due to the vibrations too small often triggering the V0C algorithm and causing false alarms. Thus, reliable data (i.e., with accuracy up to one decimal point) are only available for points located far enough from the clamped section, where the deflections are larger and the zero crossings better defined. Nevertheless, the method gives a large amount of information in a relatively compact way, and results, while noisy, are consistent with the ones from the other techniques (figure 10). Moreover, it seems not to be influenced negatively by the presence of the attachments on the extrados.

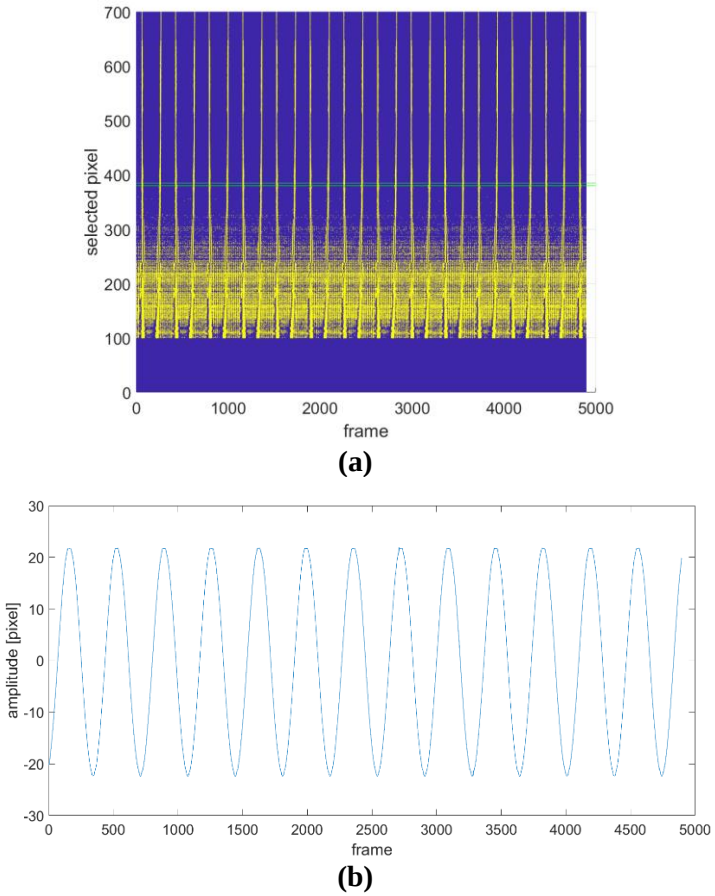


**Figure 10.** (a) Edge Detection-based Video Zero Crossing algorithm run over the pixels of the selected tract depicted in figure 6 (on the y-axis) for a constant dwelling time history. The x-axis reports the video length in terms of frames (0 to 4897). Yellow dots represent a recorded zero crossing; blue means no crossing. (b) results from the VVV algorithm applied to the y coordinates of the six-pixel-wide tract included into the two green lines in (a). Results (showed here in terms of pixels and frames) were found to be perfectly consistent in terms of frequency.

## 6. Conclusions

Results show that, under appropriate conditions and using proper arrangements, good quality time histories can be extracted from video recordings by using the techniques here proposed. In particular, it was shown by experimental results that the Marker Detection (MD) and tracking routine is successfully able to locate several targets applied to the spar frame-by-frame, returning their respective 2-dimensional time histories of displacements, or at least their projection on the focal plane. The sub-pixel accuracy of the method depends on several environmental conditions and on the specific setup deployed but reached acceptable levels for most practical uses.
Some technical considerations regarding the experimental setup were also found. For instance, the solid circle marker design (M1 and M4) performed much better than the chequered and the X-shaped ones, independently from the marker colour. While this can be a fortuitous chance, it may be probably due to the circular design, the shape of which grants strong and similar directional gradients in all directions (not only along *x*- and *y*-axes) and is rotation-invariant. However, the optical tracking algorithm proved to be quite sensitive to the chosen target frame and the exact size and position of the target window. Thus, the technique performs better when the target frame is selected so that the beam-like structure is close to its initial configuration.

Both the other benchmarked techniques, proposed respectively for the acquisition of 1-dimensional displacements (VVV) and for the definition of the instantaneous frequency along all the structure's points at once (V0C), performed well for their intended purpose, but with some caveats. If directly compared to the LDV, VVV has pixel-limited accuracy, hence it is much coarser. On the other hand, the VVV algorithm is not hampered by clipping issues, which arises in laser measurements for large

motions as the ones here investigated. It also directly measures displacements, avoiding the need to numerically integrate velocities.
The V0C accuracy increases proportionally to the displacement's amplitude but is unreliable for small vibrations and unsuited for subpixel measurements; its results are also very noisy. Nevertheless, they are consistent with time histories obtained through all the other methods and are able to compute the frequency of the vibration at any instant and at any position with a very small computational cost.

Some comparison between the three techniques were also drawn. For small displacements, VVV and MD are basically interchangeable, and VVV algorithm is more robust and does not need attached targets. For larger displacements, when the linear limit is exceeded, VVV is still viable if the level of accuracy required is not too strict and some percentage of error is accepted. For very large deflections or in the case where high accuracy is required, MD should be preferred instead, as it gives great insight into the actual curve motion of the point of interest. VVV intrinsic limitation to one direction makes it unsuited for curvilinear motions of a cantilevered beam undergoing very large oscillations; this is the same limitation of the laser Doppler velocimeter. However, this phenomenon, neglected for small amplitudes, seems to remain little even for some moderately larger deflections. Nevertheless, this aspect needs further investigation before being fully confirmed; if proved correct, this estimation error could be low enough to be acceptable for some uses for moderately large oscillations.

Overall, the major practical issues of using video processing to extract displacements time histories are the high number of fps required (in particular to avoid motion blunder, which is very deleterious for marker detection), and the accuracy resolution, which is generally lower than for other common techniques. Results depend heavily on the lighting conditions at recording; moreover, Marker Detection algorithm requires attached markers and depends strongly on their size and shape; its performance is also influenced by the selection of a proper reference frame. All the algorithms proposed can be furtherly improved in different ways. For instance, bit-plane slicing, or other image processing techniques, can be used to remove useless information from grayscale frames.

Finally, Raspberry Pi IMUs proved to be a good low-cost solution for minimally invasive measurements, as their alteration of the spar linear dynamics is almost negligible for common practical use. Effects on nonlinear dynamics, which are much more sensible, are more evident, yet significantly smaller than the ones from heavier alternatives. Therefore, they can be considered as a suitable low-cost substitute for other more expensive lightweight accelerometers, when the non-contact measurement of flexible structures is impossible or unpractical.

**Acknowledgements**
Authors would like to thank Dr Ivan Petrunin and PhD student Alessandro Pontillo for their help with the experimental setup and the Raspberry PI acquisition, respectively. First Author is thankful to the Cranfield University for the facilities provided and to the Politecnico di Torino for allowing this joint research.

## References

1. González-Cruz CA, Jauregui-Correa JC, Herrera-Ruiz G (2016) Nonlinear Response of Cantilever Beams Due to Large Geometric Deformations: Experimental Validation. Strojniški Vestn - J Mech Eng 62:187–196. https://doi.org/10.5545/sv-jme.2015.2964
2. Worden K, Tomlinson GR (2001) Nonlinearity in structural dynamics : detection, identification, and modelling. Institute of Physics
3. Shawky A, Zydek D, Elhalwagy YZ, Ordys A (2013) Modeling and nonlinear control of a flexible-link manipulator. Appl Math Model 37:9591–9602. https://doi.org/10.1016/J.APM.2013.05.003
4. Pontillo A, Hayes D, Dussart GX, et al (2018) Flexible High Aspect Ratio Wing: Low Cost Experimental Model and Computational Framework. In: 2018 AIAA Atmospheric Flight Mechanics Conference. American Institute of Aeronautics and Astronautics, Reston, Virginia
5. Platten MF, Wright JR, Cooper JE, Dimitriadis G (2009) Identification of a Nonlinear Wing Structure Using an Extended Modal Model. J Aircr 46:1614–1626. https://doi.org/10.2514/1.42024
6. Zhang W, Sun L, Yang XD, Jia P (2013) Nonlinear dynamic behaviors of a deploying-and-retreating wing with

varying velocity. J Sound Vib 332:6785–6797. https://doi.org/10.1016/J.JSV.2013.08.006
7. Dussart G, Portapas V, Pontillo A, Lone M (2018) Flight Dynamic Modelling and Simulation of Large Flexible Aircraft. In: Flight Physics - Models, Techniques and Technologies. InTech
8. Worden K (1990) Data processing and experiment design for the restoring force surface method, part I: integration and differentiation of measured time data. Mech Syst Signal Process 4:295–319. https://doi.org/10.1016/0888-3270(90)90010-I
9. Castellini P, Martarelli M, Tomasini EP (2006) Laser Doppler Vibrometry: Development of advanced solutions answering to technology's needs. Mech Syst Signal Process 20:1265–1285. https://doi.org/10.1016/j.ymssp.2005.11.015
10. Stanbrifge AB, Ewins DJ (1999) Modal Testing Using a Scanning Laser Doppler Vibrometer. Mech Syst Signal Process 13:255–270. https://doi.org/10.1006/MSSP.1998.1209
11. Castellini P, Paone N (2000) Development of the tracking laser vibrometer: Performance and uncertainty analysis. Rev Sci Instrum 71:4639. https://doi.org/10.1063/1.1319862
12. Wadhwa N, Rubinstein M, Durand F, Freeman WT (2013) Phase-based video motion processing. ACM Trans Graph 32:1. https://doi.org/10.1145/2461912.2461966
13. Chen JG, Wadhwa N, Cha Y-J, et al (2015) Modal identification of simple structures with high-speed video using motion magnification. https://doi.org/10.1016/j.jsv.2015.01.024
14. Yang Y, Dorn C, Mancini T, et al (2017) Blind identification of full-field vibration modes from video measurements with phase-based video motion magnification. Mech Syst Signal Process 85:567–590. https://doi.org/10.1016/j.ymssp.2016.08.041
15. Wahbeh AM, Caffrey JP, Masri SF (2003) A vision-based approach for the direct measurement of displacements in vibrating systems. Smart Mater Struct 12:785–794. https://doi.org/10.1088/0964-1726/12/5/016
16. Zaurin R, Necati Catbas F (2011) Structural health monitoring using video stream, influence lines, and statistical analysis. Struct Heal Monit An Int J 10:309–332. https://doi.org/10.1177/1475921710373290
17. Malatkar P, Nayfeh AH (2003) A Parametric Identification Technique for Single-Degree-of-Freedom Weakly Nonlinear Systems with Cubic Nonlinearities. Modal Anal 9:317–336. https://doi.org/10.1177/107754603030754
18. Kristan M, Leonardis A, Matas J, et al (2019) The Sixth Visual Object Tracking VOT2018 Challenge Results. Springer, Cham, pp 3–53
19. Bay H, Tuytelaars T, Gool L Van (2006) SURF: Speeded Up Robust Features. In: European conference on computer vision. pp 404–417
20. Leutenegger S, Chli M, Siegwart RY BRISK: Binary Robust Invariant Scalable Keypoints
21. Rosten E, Drummond T Fusing Points and Lines for High Performance Tracking
22. Harris C, Stephens M A COMBINED CORNER AND EDGE DETECTOR
23. Jianbo Shi, Tomasi (1994) Good features to track. In: Proceedings of IEEE Conference on Computer Vision and Pattern Recognition CVPR-94. IEEE Comput. Soc. Press, pp 593–600
24. Obdržálek D, Basovník S, Mach L, Mikulík A (2010) Detecting Scene Elements Using Maximally Stable Colour Regions. Springer, Berlin, Heidelberg, pp 107–115
25. Brown M, Lowe D Invariant Features from Interest Point Groups
26. Savitzky A, Golay MJE (1964) Smoothing and Differentiation of Data by Simplified Least Squares Procedures. Anal Chem 36:1627–1639. https://doi.org/10.1021/ac60214a047
27. Canny J (1986) A Computational Approach to Edge Detection. IEEE Trans Pattern Anal Mach Intell PAMI-8:679–698. https://doi.org/10.1109/TPAMI.1986.4767851
28. Maini R, Dr & Study and Comparison of Various Image Edge Detection Techniques